A method for estimating the spatial coherence of mid-latitude skywave propagation based on transionospheric scintillations at 35 MHz

J. F. Helmboldt[1]

[1]US Naval Research Laboratory, 4555 Overlook Ave. SW, Washington, DC 20375, USA.

Key Points:

- A method was developed to convert transionospheric scintillation measurements at 35 MHz to estimates of skywave spatial coherence.
- Data were collected with an array of antennas focused on cosmic radio sources and the CHU radio station at 35 and 7.85 MHz, respectively.
- These data demonstrated that 35 MHz scintillations can be reliably used to assess day-to-day variations in skywave spatial coherence.

Corresponding author: Joseph Helmbolt, `joseph.helmboldt@nrl.navy.mil`

Abstract

The results of a study aimed at assessing the utility of transionospheric 35 MHz scintillation measurements toward cosmic radio sources for estimating the level of spatial coherence in high frequency (HF) skywave systems are presented. This was done using an array of four antennas in southern Maryland called the Deployable Low-band Ionosphere and Transient Experiment (DLITE). Two of the antennas within a ∼350-m north/south baseline were used to monitor 35-MHz intensity variations of two bright cosmic sources, Cynus A and Cassiopeia A. The other two antennas, which were within a ∼420-m east/west baseline, recorded the 7.85 MHz skywave from the CHU radio station near Ottawa, Ontario. These HF measurements were used to quantify the level of spatial coherence by measuring the amplitudes of the cross correlation of the two antennas' recorded voltages relative to the received power, which were typically ∼0.5–0.9, but occasionally near zero. A method was developed to estimate the expected cross-correlation amplitude based on the 35-MHz scintillations. This method assumes the case of weak scattering, which is generally appropriate for mid-latitudes, and that the irregularity distribution follows that of the background electron density. These calculations typically captured the day-to-day variations in spatial coherence quite well (correlation coefficient $r \simeq 0.6$) while only marginally reproducing hour-to-hour variations ($r \simeq 0.2$). Thus, this method holds promise as an economical and passive means to assess the spatial coherence expected for skywave propagation within a given mid-latitude region.

1 Introduction

For just over a century, refraction of medium frequency (MF; 0.3–3 MHz) and high frequency (HF; 3–30 MHz) radio waves within the ionosphere has offered a reasonably low-loss (especially at night) pathway for over-the-horizon (OTH) communications and radar-based surveillance. This so-called "skywave" propagation offered one of the first means of global wireless radio communication. Even in an age of replete with satellite-based systems, skywave HF comms and OTH radars continued to be exploited as economical means for long-range transmissions and surveillance of large areas from far away.

The ionosphere is not a static medium, however, and so this approach is not without drawbacks. Disturbances and irregularities on scales from a few meters to thousands of kilometers occur and can cause various deleterious effects on skywave systems. Because they are comparable to the Fresnel scale for ground-based HF systems, km-scale irregularities can be especially problematic. Such irregularities cause phase and intensity variations that can, for instance, broaden Doppler signatures within OTH radars and, in some cases, cause a complete loss of temporal or spatial coherence. The latter is of particular concern for systems that rely on arrays of receiving antennas since they require at least some level of coherence among the array elements. Thus, having a detailed assessment of the ionospheric coherence length within a given region is important for both site selection and design of array-based skywave systems.

Such an assessment is not always practical and/or economical with shortwave systems, especially if coverage within a relatively large region is desired. At low and high latitudes, irregularity activity is typically high enough that satellite-based microwave beacons, e.g., Global Positioning System (GPS) signals, can be used to estimate parameters such as the coherence length and extrapolate to the HF regime. Consequently, GPS scintillations have been used for decades to study ionospheric irregularities within these regions (for a review, see Kintner et al. (2007)).

At mid-latitudes, irregularity activity tends to be quite low by comparison. Because the impact of these structures is stronger the closer the operating frequency is to the ionospheric plasma frequency (usually ∼1–10 MHz), scintillations at mid-latitudes are rarely visible at microwave frequencies. At lower frequencies ($\lesssim$100 MHz), scintillations are nearly always present, but there are few if any satellite-based transmitters within this frequency

regime. Cosmic radio sources offer an alternative as many of these objects have spectra that increase in intensity at lower frequency (due to, e.g., synchrotron emission). Indeed, there is a growing body of work of radio telescope-based measurements used to study ionospheric disturbances toward cosmic radio sources (e.g., Jacobson and Erickson (1992); Cohen and Röttgering (2009); Helmboldt et al. (2012); Loi et al. (2015); Helmboldt and Hurley-Walker (2020)). In particular, Mevius et al. (2016) demonstrated that scintillations at low frequencies toward bright cosmic radio sources are always present. Because interferometers are often used within radio astronomy for high angular resolution imaging, especially at lower frequencies, the coherence length is an important quantity for telescope design and siting as well. This is especially true given recent efforts to push to lower frequencies in search of signatures of the so-called Cosmic Dawn, which are related to a reduction in emission from neutral hydrogen in the early universe due to photoionization by the first starts (e.g., DiLullo et al. (2020)).

In an effort to build on successes with radio astronomy-based ionospheric measurements while circumventing the portability limitations of large radio telescopes, a new low-cost telescope array, optimized for ionospheric remote sensing, was recently developed. This Deployable Low-band Ionosphere and Transient Experiment (DLITE) consists of four antennas that monitor a small number of exceptionally bright cosmic radio sources at 35 MHz for ionospheric variations in both intensity and phase (Helmboldt et al., 2021). The study presented here was focused on using a DLITE array in southern Maryland in a novel mode to assess the utility of transionospheric 35 MHz scintillation measurements to characterize the expected spatial coherence of an HF skywave signal. To test this, the 7.85 MHz carrier wave of the CHU radio station near Ottawa, Ontario received at the Maryland site was also recorded and analyzed. The experimental setup and results of a data collection campaign from Oct./Nov. 2020 are detailed in Sec. 2 while the method for converting 35-MHz scintillation measurements to 7.85 coherence estimates is described in Sec. 3. Results are summarized and discussed in Sec. 4.

2 Experiment Design and Observations

Data were obtained within a novel collection mode utilizing a DLITE system deployed near Pomonkey, Maryland (DLITE-POM for short). A thorough description of the DLITE system and the methods developed to analyze the data it produces is given by Helmboldt et al. (2021). In brief, DLITE is a radio telescope array of four antennas, which were originally designed for the Long Wavelength Array (LWA) project (Taylor et al., 2012; Ellingson et al., 2013). They are bowtie-shaped, bent dipole antennas with active baluns that make them sky noise-dominated (by 6 dB or more) in the 20-80 MHz range (Hicks et al., 2012). DLITE employs these antennas as an interferometer connected to a digital backend composed of mostly commercial off-the-shelf (COTS) parts, including widely used Ettus-brand software defined radios. This backend continuously cross-correlates all six unique baselines within the array. To avoid the relatively large number of antennas needed for beam forming with phased arrays, DLITE uses time and frequency difference of arrival (TDOA and FDOA) to resolve individual cosmic radio sources from one another. This is enabled by relatively long baselines (∼200–500 m) and large bandwidth (∼6–10 MHz).

DLITE-POM was deployed in the summer/fall of 2019, in part to support the Space Measurement of a Rocket-released Turbulence (SMART) experiment (Ganguli et al., 2019; Fletcher et al., 2020). With help from colleagues at the University of New Mexico, a second array was established at the site of the Very Large Array (VLA) near Datil, New Mexico by repurposing existing but dormant LWA antennas. A third array was deployed at Malabar Annex Space Force Base near Melbourne, Florida in Nov. 2021 in cooperation with the 45$^{\text{th}}$ Space Wing.

For the SMART experiment, methods were developed to use DLITE as a scintillometer. Considering various factors, it was found that the optimum band for scintillation measurements is 30–40 MHz. These rely on the generation of TDOA/FDOA images from each of the array's six baselines. For each baseline, a particular cosmic source has a predictable TDOA and FDOA. For the fractional bandwidth used by DLITE (∼24%), the equivalent resolution on the sky for TDOA and FDOA are the same for an integration time of about one hour. In practice, windowing reduces the temporal resolution to ∼30 minutes. Within these images, scintillations create a plateau-like artifact in the FDOA direction only, the magnitude of which is $= \sigma_I/\sqrt{N_t}$, where σ_I is the intensity standard deviation and N_t is the number of time steps used to generate the TFOA/FDOA image. Thus, the peak intensity relative to this artifact can be used to measure the S_4 scintillation index, which is the ratio of σ_I to the mean intensity. Combining the S_4 index with the observing geometry yields the irregularity index, C_kL, which is proportional to the vertically integrated electron density variance.

According to Rino (1979); Carrano et al. (2019); Helmboldt et al. (2021), for frequencies well above the plasma frequency, the S_4 index is related to C_kL by

$$S_4 = \frac{\sigma_I}{I} \tag{1}$$

$$\sigma_I^2 = I^2 \frac{C_k L}{\sin e}(r_e\lambda)^2 \left(\frac{2\pi}{1000}\right)^{2\nu+1} \left(\frac{z_R\lambda}{2\pi \sin e}\right)^{\nu-0.5} \frac{\wp(\nu)F_S(\nu)}{D_S} + \sigma_{sys}^2 \tag{2}$$

$$F_S(\nu) = \frac{\Gamma(1.25+\nu/2)}{2^{\nu+0.5}\sqrt{\pi}\Gamma(\nu/2+0.25)(\nu-0.5)} \tag{3}$$

with all quantities specified in MKS units. In equation (2), r_e is the classical electron radius, z_R is the irregularity height, σ_{sys} is the system noise (including external/sky noise), and $\wp$ is a geometric and propagation factor that depends on the orientation of the irregularities relative to the line of sight. For mid-latitudes, it is generally a good assumption that the irregularities are aligned along magnetic field lines with major/minor axis ratios of about 10:1, which is what is assumed for DLITE analysis. The irregularities are also assumed to be at a height of 300 km, but the dependence on assumed height is relatively weak ($\propto z_R^{0.85}$). The shape of the irregularity spectrum is represented by ν, which is assumed to be 1.35 to approximate Kolmogorov turbulence (Tatarskii, 1961). The observing wavelength is λ, and e is the elevation angle of the line of sight. The factor D_S is unique to DLITE and accounts for the fact that none of the observed A-Team sources are point-like. The derivation of this value per source is described by Helmboldt et al. (2021).

For this study, the DLITE-POM array was run in a novel mode where only two antennas, those within a relatively long north/south baseline (∼350 m), were cross-correlated in the normal way and used to generate TDOA/FDOA images for scintillometry at 35 MHz. The other two antennas form a ∼420-m east/west baseline and were used to record raw complex voltages at 7.85 MHz with 2.5 kHz of bandwidth to monitor the skywave propagated signal from CHU. The linear polarization voltages at 7.85 MHz were converted to right- and left-handed circular polarization (RHCP and LHCP, respectively), and cross-correlated after the fact with a coherent integration time of 1.2 s. We note that even in this novel mode, all eight channels of the system (four antennas, two polarizations each) were synched to the same 10 MHz reference and pulse per second signal during all collections, as usual (see Helmboldt et al. (2021)). Collections in this mode were performed every day from 2 Oct. through 1 Nov. 2020 from 17–23 UT each day (except 1 Nov., for which data was collected 18–24 UT) to maximize the time that the 7.85 MHz CHU signal was detectable from Pomonkey and when the two brightest cosmic 35 MHz sources, Cygnus A and Cassiopeia A (Cyg A and Cas A), were visible.

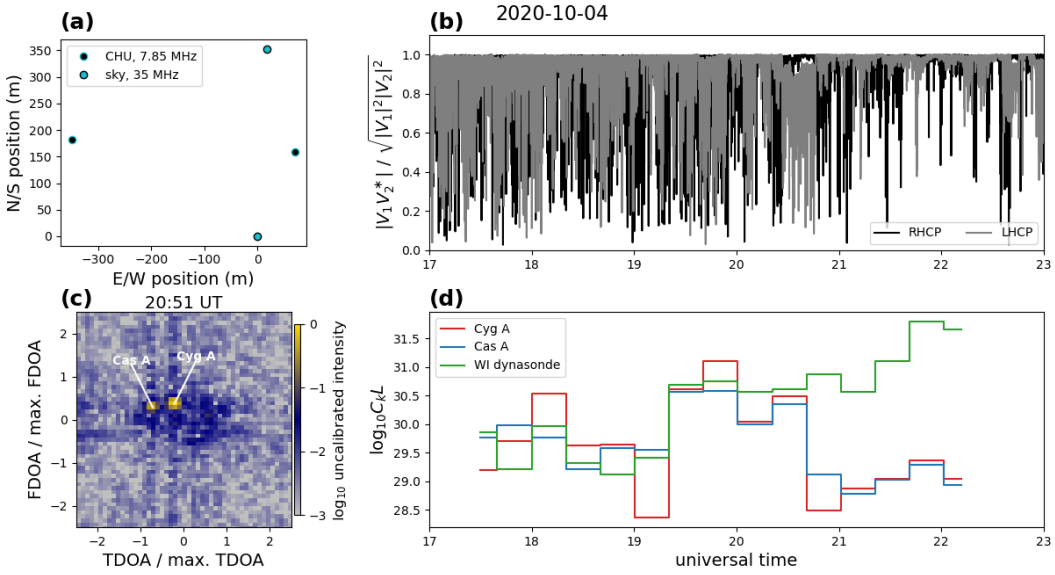

Figure 1. An example of the data products generated from the observing campaign. (a) The layout of the DLITE-POM antennas. The antennas used for 35-MHz sky observations are represented by cyan dots; those used to record the 7.85 MHz CHU skywave are represented by black dots. (b) The cross-correlation amplitude between the two antennas used to record the CHU skywave as a function of time within 1.2-s integrations. Right- and left-hand circular polarization (RHCP and LHCP) are plotted in black and gray, respectively. (c) A time and frequency difference of arrival (TDOA and FDOA) image of the sky at 35 MHz from the data collected with the north/south baseline shown in panel (a). The locations of the two bright sources Cyg A and Cas A are indicated. (d) Time series of the C_kL irregularity index extracted from the 35 MHz data for Cyg A (red) and Cas A (blue) as well as estimates from parameters take from the Wallops Island (WI) dynasonde (green; see Sec. 2).

This observing mode and its data products are illustrated in Fig. 1 which shows for 4 Oct. 2020 (a) the antenna layout, including which antennas were used for which measurements, (b) the cross-correlation amplitude of the CHU 7.85 MHz signals relative to the received power, (c) one of 15 TDOA/FDOA images of the sky at 35 MHz, and (d) C_kL derived from Cyg A (red) and Cas A (blue). Within panel (b), one can see the plateau-like FDOA artifacts reference above (in blue) used to characterize the level of scintillations. The resulting C_kL values are mostly higher prior to 21 UT after which they drop somewhat, although with some level of disagreement between the two sources. Likewise, the spatial coherence of the 7.85 MHz signal tended to be lower prior to 21 UT and higher afterward (i.e., the coherence should be lower when C_kL is larger).

Following the analysis of Helmboldt and Zabotin (2022), parameters were also obtained from the Wallops Island (WI) dynasonde radar system, which is ∼160 km southeast of Pomonkey. Automatically generated parameters that characterize the peak plasma frequency, peak height, scale height, and km-scale irregularity spectrum for the E- and F-regions separately were used. Helmboldt and Zabotin (2022) showed that combining these parameters while assuming the irregularities follow the N_e profile with Chapman layers per region yielded estimates of C_kL that were in good agreement with measurements made with DLITE-POM. The green curve in Fig. 1d shows C_kL computed in this way, averaged within the same time intervals used for the DLITE-POM measurements. One can see that they agree rather well up until just before 21 UT, where the DLITE C_kL drops and the WI values rise somewhat. This is in contrast with the CHU 7.85 MHz signal, which becomes more spatially coherent during this time, implying that there may have been somewhat localized irregularity activity near WI at that time.

3 Spatial Coherence Calculations

This section provides details regarding the model used to compute estimates of spatial coherence constrained with DLITE-based C_kL measurements. This is a modified version of the single-layer model published by Rino (1979), and it is therefore refer to as the MR79 model for short. The original model was designed for transionospheric propagation of radio signals at frequencies much higher than the plasma frequency. The MR79 version contains additional terms meant to adapt it to skywave propagation where the signals do not leave the bottom-side of the ionosphere and are at frequencies larger than, but similar to, the plasma frequency.

3.1 Model Derivation

The derivation of the model published by Rino (1979) begins with a relationship between the change in phase of a radio signal, $\delta\phi$, due to a perturbation in the ionospheric electron density, ΔN_e, which assumes $f \gg f_p$, where f_p is the plasma frequency $= c\sqrt{N_e r_e/\pi}$. More generally, $\delta\phi$ can be related to a change in the index of refraction, $N = \sqrt{1-(f_p/f)^2}$, namely

$$\delta\phi = \frac{2\pi}{\lambda}\int_0^\infty \Delta N ds \tag{4}$$

where ds is along a particular line of sight/propagation path. In the weak scattering case, the change in N is relatively small, and equation (5) can be approximated as

$$\delta\phi \simeq -r_e\lambda\int_0^\infty \frac{\Delta N_e}{N} ds \tag{5}$$

In this context, weak scattering refers to irregularity-driven changes in the electron density, ΔN_e, that are small enough that the approximation given in equation (5) is still

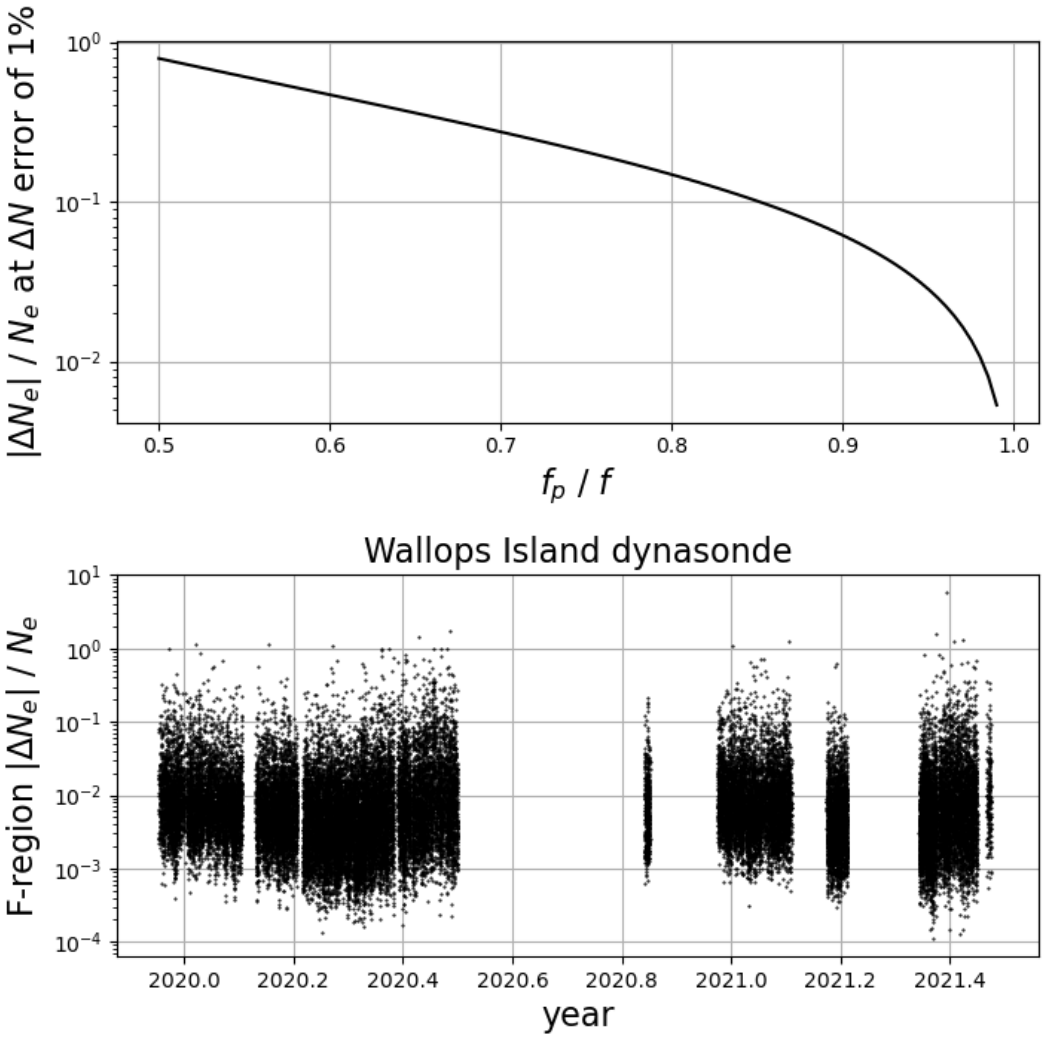

Figure 2. Upper: The relative standard deviation in the electron density, $|\Delta N_e|/N_e$, that causes an error of 1% for the resulting change in the index of refraction, ΔN, calculated from the approximation in equation (6) versus the ratio of the plasma frequency to the observing frequency. Lower: A time series of estimates of $|\Delta N_e|/N_e$ from F-region irregularity parameters measured with the dynasonde system near Wallops Island, Virginia

valid. The upper panel of Fig. 2 shows the value of $|\Delta N_e|/N_e$ that will cause this approximation to be off by 1% as a function of f_p/f. From this curve, one can see that for $f_p/f < 0.9$, relative N_e deviations of up to around 7% qualify as weak within this context. For lower f_p/f ratios, that limit can be much higher (e.g., ∼80% at $f_p/f = 0.5$). Following the analysis presented in Helmboldt and Zabotin (2022), irregularity parameters measured with the WI dynasonde were used to estimate the F-region $|\Delta N_e|/N_e$ from Dec. 2019 through Jun. 2021, and the results are plotted in the lower panel of Fig. 2. The vast majority of these estimates (97%) are below 7%. Note that for $f \simeq f_p$, this approximation cannot hold, which is why vertical sounders like the WI dynasonde must be treated differently. For a thorough discussion of this special case, see Zabotin and Wright (2001).

For $f \gg f_p$, $N \simeq 1$ everywhere, and equation (5) is the same as equation (1) of Rino (1979). For skywave propagation, this same assumption cannot be made. However, equation (5) illustrates that irregularities near the reflection height where N is at a minimum within the propagation path will have an outsized impact. Thus, even though irregularities may be distributed throughout the ionosphere, in this case, their impact can be approximated by assuming a single layer near the reflection height since those carry the largest weight. In this case, the value of N in the integrand of equation (5) can be fixed at $\sqrt{1-(f_{p,max}/f)^2}$, where $f_{p,max}$ is the plasma frequency at the reflection height, and moved outside the integral.

This implies that the relationship derived by Rino (1979) between the phase variance/covariance and the ΔN_e power spectrum can be adapted to be appropriate for skywave propagation by dividing by a factor of $1-(f_{p,max}/f)^2$ (i.e., N^2_{min}). Furthermore, for a virtual mirror approximation, $f_{p,max}/f \simeq \cos\theta$, where θ is the zenith angle of the propagation vector, and so multiplying by $\csc^2\theta$ will have a similar effect. Additionally, the signal does not propagate through the full ionosphere, and so only part of the irregularity distribution contributes to the phase variance/covariance. As supported by the results of Helmboldt and Zabotin (2022), one can assume that the irregularities follow the N_e distribution. The HF propagation simulator of Nickisch et al. (2012) also makes this same assumption. It then follows that the equations from Rino (1979) can be scaled by a factor $F_e = \left(\int_0^{h_{max}} N_e^2 dz\right)\left(\int_0^{\infty} N_e^2 dz\right)^{-1}$, where h_{max} is the reflection height. This can be calculated numerically using a specified N_e profile. Finally, for skywave propagation, the irregularity layer is effectively traversed twice for each "hop" of the signal, implying that an additional factor of $2N_{hop}$ must also be included.

Taking into account the modifications described above, the correlation function of phase variations within the MR79 model is given by

$$R_{\delta\phi}(r_{eff}) = C' \left|\frac{r_{eff}}{2q_0}\right|^{\nu-1/2} \frac{K_{\nu-1/2}(q_0 r_{eff})}{2\pi\Gamma(\nu+1/2)} \tag{6}$$

$$C' \equiv \left[2N_{hop}F_e \csc^2\theta\right] G r_e^2 \lambda^2 \sec\theta \left(\frac{2\pi}{1000}\right)^{2\nu+1} C_k L \tag{7}$$

where the terms within the first set of brackets in the definition of C' are the new ones added here, and the remainder are from equation (12) of Rino (1979). The G term is a geometrical factor described by Rino (1979), which depends on the azimuth of the propagation direction. The quantity $q_0 = 2\pi/L_0$, where L_0 is the outer scale, usually assumed to be about 30 km (Nickisch et al., 2012). The spectral shape ν is the same as that discussed in Sec. 2. This gives the phase covariance for two locations with an effective one-dimensional separation of r_{eff}, which takes into account the irregularity orientations and shapes as defined by Rino (1979). For the two antennas at DLITE-POM used to collect 7.85 MHz CHU data and the geometry of the propagation path (see Sec. 3.2), $r_{eff} \simeq 220$ m.

The phase of the cross correlated signal will have a variance given by the structure function, which is the variance in the difference in phase, $\Delta\phi$, between to points separated by r_{eff}. Since the antennas used are significantly closer together than the outer scale, the scale-free approximation can be used, which is given by Rino (1979); Carrano et al. (2019) and modified here to be

$$\sigma^2_{\Delta\phi} \simeq C' \frac{2\Gamma(3/2-\nu)}{2\pi\Gamma(\nu+1/2)(2\nu-1)2^{2\nu-1}} r_{eff}^{2\nu-1} \tag{8}$$

which is valid for $1/2 < \nu < 3/2$. The amplitude of the cross correlated signal will then be reduced by a factor of $\exp(-\sigma^2_{\Delta\phi}/2)$. This can be measured directly by normalizing

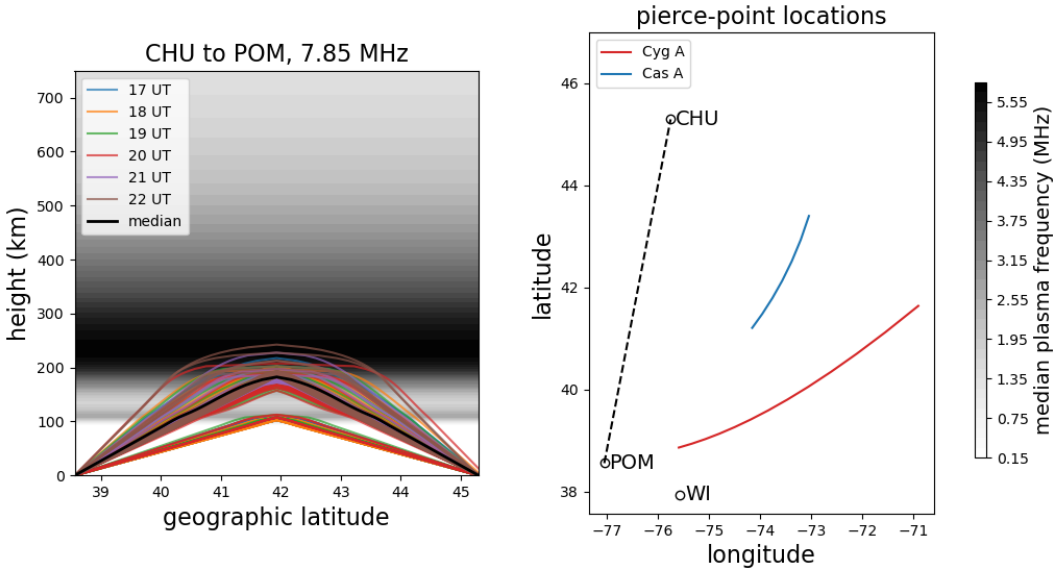

Figure 3. Left: The most likely ray path per hour during each collection date and time interval using a background ionosphere specified by the International Reference Ionosphere, constrained by parameters from the digisonde system at Wallops Island (WI). Each ray is color-coded by universal time. The grayscale image in the background is the median plasma frequency profile among all the collection dates/times. The black curve is the most likely ray path through this median profile. Right: Ionospheric pierce points at an altitude of 300 km from Pomonkey (POM) toward Cyg A (red) and Cas A (blue) during the data collections relative to the locations of the CHU radio station and the WI dynasonde. The path from CHU to POM is traced with a black dashed line.

the amplitude of the cross correlated voltages by the square root of the product of the received power (i.e., auto-correlation) at each antenna averaged over the same coherent integration time (see Fig. 1b). Thus, C_kL values measured using 35 MHz observations of Cyg A and Cas A and/or dynasonde-based estimates of C_kL can be used with estimates of F_e and θ to compute expected cross-correlation amplitudes and compared with observations.

3.2 Observational Tests

To estimate values of θ and F_e for the Oct./Nov. 2020 data collections, the International Reference Ionosphere (IRI) (Bilitza et al., 2014) constrained with parameters from the digisonde system near Wallops Island, Virginia was used to generate vertical profiles (5-km spacing) at one-hour intervals throughout the collection period. Using a simple ray tracing algorithm, the most likely signal path (with $N_{hop} = 1$) between CHU and DLITE-POM at the transmitted frequency of 7.85 MHz was estimated. These ray paths are plotted in the left panel of Fig. 3, color-coded by universal time. The median plasma frequency profile is shown in the background as a grayscale image.

While there are a few ray paths that only propagate within the E-region due to occasional sporadic-E, the vast majority travel through the lower portion of the F-region, usually well below the peak height. There is also not a clear trend with universal time, although the maximum heights of the 19 and 20 UT rays tend to be somewhat lower. The black curve within the figure shows the most likely path through the median N_e pro-

file, which also appears to be a fair representation of the typical path for all dates and times. For simplicity, the values of θ and F_e for this ray were used for all dates and times, which are 62.0° and 0.037, respectively. Here, it was assumed that θ is the complement of the initial elevation angle of the ray path. Assuming $\nu = 1.35$, it follows from equations (7)–(8) that $\sigma^2_{\Delta\phi} = 8.54 \times 10^{-32} C_k L$ in this case.

To compare with the DLITE-based $C_k L$ calculations, the mean observed 7.85 MHz cross-correlation amplitude was computed within each time interval used to calculate $C_k L$, which are spaced by ∼20 minutes. This was done by coherently averaging the complex cross correlations within each of these intervals, and then computing the amplitude of the result. As before (e.g., Fig. 1b), these cross-correlation amplitudes were then normalized by the mean received power within the same interval. The results are plotted as a function of time for each date in Fig. 4 for RHCP (black) and LHCP (gray). Horizontal black dotted lines indicate the value where $\sigma_{\Delta\phi} = 1$, which represents the case where the coherence length is equal to r_{eff} for the two DLITE antennas (approximately 220 m). Time series calculated with $C_k L$ values derived from Cyg A and Cas A are also plotted in red and blue, respectively.

While there is obviously not a one-to-one correspondence between the observed and estimated values, the DLITE-based values generally show the same level of incoherence as the data per day with a few exceptions (e.g., 26 and 28 Oct.). One should also note that the observed amplitudes will never be as close to unity as the low-$C_k L$ instances predict due to noise that is not correlated between the two antennas. Still, the correlation coefficient, r, between the observed values and the DLITE-based calculations is 0.2. This is not particularly strong, but significant nonetheless. To confirm this, the DLITE-based values were randomly resorted and the correlation coefficient was recalculated one hundred times. Among these, the 99$^{\text{th}}$ percentile was 0.1. In contrast, if the daily median values are compared, r increase to 0.6, which is consistent with the qualitative assessment above that the DLITE-based calculations reproduce the observed day-to-day variations better than the shorter timescale changes.

WI dynasonde-based values for the cross-correlation amplitude are also plotted in Fig. 4 (in green) but are not well correlated with the observed values with $r = 0.1$. Likewise, the correlation coefficient between the dynasonde-based $\log_{10} C_k L$ values and those from either Cyg A or Cas A was also 0.1. However, the daily median values of $\log_{10} C_k L$ were well correlated between the dynasonde and DLITE with $r \simeq 0.3$–0.4, similar to what was found within the longer term study of Helmboldt and Zabotin (2022). Similarly, comparing the daily median values for the 7.85 MHz cross-correlation amplitude between the observations and dynasonde-based calculations gives $r \simeq 0.4$. This implies that while the WI-measured irregularity activity did not follow the same hour-by-hour pattern as those observed with DLITE, either at 7.85 or 35 MHz, the general level of activity per day was similar.

4 Discussion and Conclusions

The results presented here show that in the weak scattering case, which is the norm at mid-latitudes, the relatively simple MR79 model can be used to convert vertically integrated scintillation measurements at 35 MHz to estimates of skywave signal spatial coherence within the same region. This was demonstrated using measurements of the cross-correlation of a 7.85 MHz skywave signal between two antennas with an effective separation of ∼220 m. While the coherence between the two is typically quite high, there are several instances where it drops low enough to infer that the coherence length was $\lesssim$220 m. This is true of both the direct observations and the values calculated based on 35-MHz scintillations. This illustrates the potential utility of such scintillation measurements for applications such as site selection/system design for skywave systems that em-

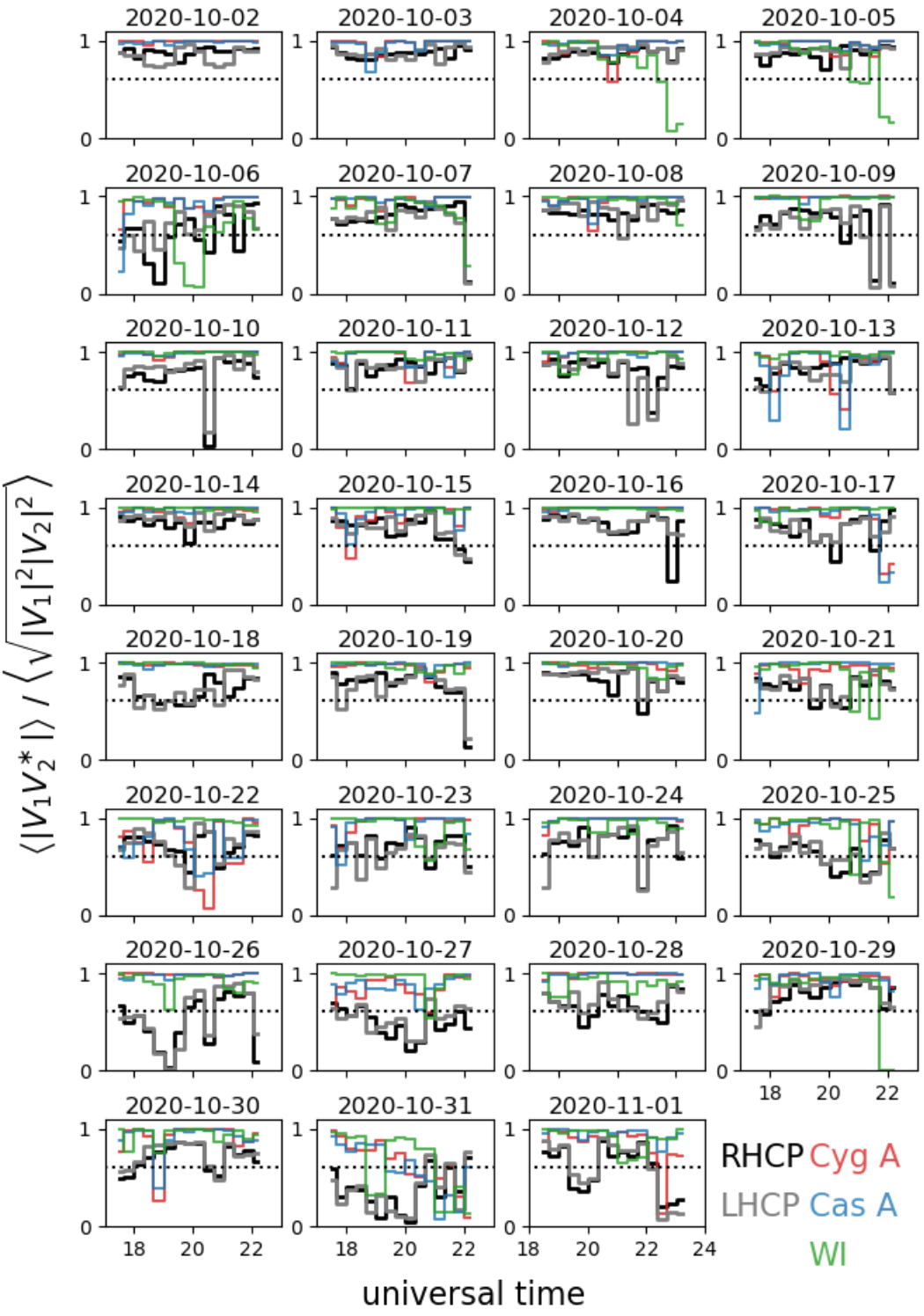

Figure 4. Time series of 7.85 MHz cross-correlation amplitudes within intervals of ∼20 minutes per day of the campaign. Observed values are plotted in black and gray for right- and left-hand circular polarization, respectively. Estimates from $C_k L$ values derived from 35-MHz observations of Cyg A and Cas A are plotted in red and blue, respectively, and those derived from Wallops Island (WI) dyansonde parameters are plotted in green. The value at which the variance in the differential phase is unity, i.e., $\sigma_{\Delta\phi} = 1$, is represented by a horizontal black dotted line within each panel.

ploy spatial arrays of antenna, even at mid-latitudes where scattering is often relatively weak.

This main result, however, is not without caveats. The agreement between the 7.85 MHz skywave observations and estimates based on DLITE scintillation measurements are significantly but weakly correlated. While the general level of spatial coherence per day is often reproduced relatively well, the agreement per time interval is not as good. This is likely due in part to the physical separation between the locations probed by the 7.85 and 35 MHz observations, which is illustrated in the right panel of Fig. 3. The fact that the results based on the WI dynasonde do not correlate significantly on an hourly basis with the 7.85 MHz observations is somewhat consistent with this since it is at a lower latitude than either the midpoint between CHU and Pomonkey or the ionospheric pierce points associated with Cyg A or Cas A.

In addition, the results for Cyg A and Cas A often do not agree, and the C_kL values derived from each typically differ by a factor of $\sim$2 (Helmboldt et al., 2021). That being said, the difference between the Cyg A and Cas A calculations is often smaller than the difference between either of them and the observed 7.85 MHz cross-correlation amplitude as evidenced by the plots in Fig. 4. Thus, there must limitations to this approach that go beyond spatial variations in C_kL within the region. These may include the assumption of single values for θ and F_e as well as the fact that the lines of sight toward the cosmic sources are moving while the HF ray path is essentially fixed. Other assumptions within the model calculations likely also play a role, including those used to convert dynasonde parameters into C_kL.

Despite limitations, these results represent a promising step toward a better understanding of mid-latitude km-scale irregularities and a capability for estimating their impact on HF skywave systems. DLITE scintillation measurements in particular are based on observations of naturally occurring, cosmic radio sources, and thus have the potential to yield a completely passive method for assessing HF skywave channel quality within a given mid-latitude region.

Acknowledgments

Digisonde parameters were obtained from the Global Ionosphere Radio Observatory (`https://giro.uml.edu`). Derived DLITE data products used within this publication are available via the Long Wavelength Array (LWA) data archive at `https://lda10g.alliance.unm.edu/~dlite/chu`. Dynasonde parameters used within this study can be obtained via SQL database query accessible at `http://surf.colorado.edu/login.dcc`. Instructions on how to obtain an account for database access are provided there. International Reference Ionosphere software was obtained from `https://irimodel.org`. Development and testing of the DLITE system were supported by the Defense Advanced Research Agency (DARPA) Space Environment Exploitation (SEE) program. Research performed for this project was supported by the Naval Innovative Science and Engineering (NISE) program at the U.S. Naval Research Laboratory.

References

Bilitza, D., Altadill, D., Zhang, Y., Mertens, C., Truhlik, V., Richards, P., ... Reinisch, B. (2014, Feb). The International Reference Ionosphere 2012 - a model of international collaboration. *Journal of Space Weather and Space Climate*, *4*, A07. doi: 10.1051/swsc/2014004

Carrano, C. S., Groves, K. M., & Rino, C. L. (2019). On the relationship between the rate of change of total electron content index (roti), irregularity strength (ckl), and the scintillation index (s4). *Journal of Geophysical Research: Space Physics*, *124*(3), 2099-2112. Retrieved from `https://`

agupubs.onlinelibrary.wiley.com/doi/abs/10.1029/2018JA026353 doi: https://doi.org/10.1029/2018JA026353

Cohen, A. S., & Röttgering, H. J. A. (2009, August). Probing Fine-Scale Ionospheric Structure with the Very Large Array Radio Telescope. *Astron. J.*, *138*, 439-447. doi: 10.1088/0004-6256/138/2/439

DiLullo, C., Taylor, G. B., & Dowell, J. (2020). Using the long wavelength array to search for cosmic dawn. *Journal of Astronomical Instrumentation*, *09*(02), 2050008. doi: 10.1142/S2251171720500087

Ellingson, S. W., Taylor, G. B., Craig, J., Hartman, J., Dowell, J., Wolfe, C. N., ... Weiler, K. W. (2013, May). The LWA1 Radio Telescope. *IEEE Transactions on Antennas and Propagation*, *61*, 2540-2549. doi: 10.1109/TAP.2013.2242826

Fletcher, A. C., Crabtree, C., Huba, J., Ganguli, G., & Siefring, C. (2020). Early time evolution of turbulence in the space environment by neutral beam injection. *Journal of Geophysical Research: Space Physics*, *125*(1), e2019JA027587. (e2019JA027587 10.1029/2019JA027587) doi: https://doi.org/10.1029/2019JA027587

Ganguli, G., Crabtree, C., Fletcher, A. C., Rudakov, L., Richardson, A. S., Huba, J., ... Lewis, C. D. (2019). Understanding and harnessing the dual electrostatic/electromagnetic character of plasma turbulence in the near-earth space environment. *Journal of Geophysical Research: Space Physics*, *124*(12), 10365-10375. doi: https://doi.org/10.1029/2019JA027372

Helmboldt, J. F., & Hurley-Walker, N. (2020). Ionospheric irregularities observed during the gleam survey. *Radio Science*, *55*(10), e2020RS007106. Retrieved from https://agupubs.onlinelibrary.wiley.com/doi/abs/10.1029/2020RS007106 (e2020RS007106 10.1029/2020RS007106) doi: https://doi.org/10.1029/2020RS007106

Helmboldt, J. F., Lazio, T. J. W., Intema, H. T., & Dymond, K. F. (2012, February). High-precision measurements of ionospheric TEC gradients with the Very Large Array VHF system. *Radio Science*, *47*, 0. doi: 10.1029/2011RS004883

Helmboldt, J. F., Markowski, B. B., Bonanno, D. J., Clarke, T. E., Dowell, J., Hicks, B. C., ... Taylor, G. B. (2021). The deployable low-band ionosphere and transient experiment. *Radio Science*, *56*(7), e2021RS007298. (e2021RS007298 2021RS007298) doi: https://doi.org/10.1029/2021RS007298

Helmboldt, J. F., & Zabotin, N. (2022). An observed trend between mid-latitudes km-scale irregularities and medium-scale traveling ionospheric disturbances. *Radio Science*, *57*(5), e2021RS007396. doi: https://doi.org/10.1029/2021RS007396

Hicks, B. C., Paravastu-Dalal, N., Stewart, K. P., Erickson, W. C., Ray, P. S., Kassim, N. E., ... Weiler, K. W. (2012, October). A Wide-Band, Active Antenna System for Long Wavelength Radio Astronomy. *Publications of the Astronomical Society of the Pacific*, *124*, 1090-1104. doi: 10.1086/668121

Jacobson, A. R., & Erickson, W. C. (1992, April). A method for characterizing transient ionospheric disturbances using a large radiotelescope array. *Astron. Astrophys.*, *257*, 401-409.

Kintner, P. M., Ledvina, B. M., & de Paula, E. R. (2007). Gps and ionospheric scintillations. *Space Weather*, *5*(9). Retrieved from https://agupubs.onlinelibrary.wiley.com/doi/abs/10.1029/2006SW000260 doi: https://doi.org/10.1029/2006SW000260

Loi, S. T., Murphy, T., Cairns, I. H., Menk, F. W., Waters, C. L., Erickson, P. J., ... Williams, C. L. (2015, May). Real-time imaging of density ducts between the plasmasphere and ionosphere. *Geophysical Research Letters*, *42*(10), 3707-3714. doi: 10.1002/2015GL063699

Mevius, M., van der Tol, S., Pandey, V. N., Vedantham, H. K., Brentjens, M. A., de Bruyn, A. G., ... Zaroubi, S. (2016). Probing ionospheric structures using the

lofar radio telescope. *Radio Science*, *51*(7), 927-941. Retrieved from `https://agupubs.onlinelibrary.wiley.com/doi/abs/10.1002/2016RS006028` doi: https://doi.org/10.1002/2016RS006028

Nickisch, L. J., St. John, G., Fridman, S. V., Hausman, M. A., & Coleman, C. J. (2012). Hicirf: A high-fidelity hf channel simulation. *Radio Science*, *47*(4). doi: https://doi.org/10.1029/2011RS004928

Rino, C. L. (1979). A power law phase screen model for ionospheric scintillation: 1. weak scatter. *Radio Science*, *14*(6), 1135-1145. doi: https://doi.org/10.1029/RS014i006p01135

Tatarskii, V. I. (1961). *Wave Propagation in Turbulent Medium.* McGraw-Hill.

Taylor, G. B., Ellingson, S. W., Kassim, N. E., Craig, J., Dowell, J., Wolfe, C. N., ... Wood, D. L. (2012, December). First Light for the First Station of the Long Wavelength Array. *Journal of Astronomical Instrumentation*, *1*, 50004. doi: 10.1142/S2251171712500043

Zabotin, N. A., & Wright, J. W. (2001, July). Ionospheric irregularity diagnostics from the phase structure functions of MF/HF radio echoes. *Radio Science*, *36*(4), 757-771. doi: 10.1029/2000RS002512